A Simultaneous Multiple Space-/Time-Scale Formulation of Fluid Flow Problems with Application to Combustion Thermoacoustics

C. Balaji[1] and S. R. Chakravarthy*[1]

[1] Department of Aerospace Engineering, Indian Institute of Technology Madras
Chennai, India, 600036
* Corresponding author: src@iitm.ac.in

A generalized formulation of combustion-acoustic coupling at simultaneous multiple time- and length-scales is presented. The compressible Navier Stokes equations are expanded about the mean flow Mach number (M) and the ratio of flow and acoustic length scales (h/L). This results in equations separating into the one governing the incompressible base flow evolving at longer time and shorter length scale and the other, the acoustics evolving at shorter time and longer length scale. Explicit coupling terms, the dilatation of the base flow as a source of acoustic energy and the acoustic Reynolds stress (ARS) as the source to base flow momentum are identified. Simulations are carried out in a dump combustor with varying step locations and the behaviour reported earlier in the literature are observed. The flame acoustic system, initially in the multi-time/length scale regime, is shown to evolve towards the single-time/multi-length scale regime as a result of the coupling. The ARS is shown to play a dominant role in curling up the flame and making it a compact acoustic source during this evolution. The system approaches the single time multiple length scale regime much faster with increase in the flow velocity. Acoustic damping, when accounted for, limits the acoustic amplitude and flame/vortex roll-up, and its subsequent shedding are predicted by the coupled nonlinear system.

1 Introduction

It is well known that there are many practical fluid flow problems of either multiple time scales or multiple length scales or both. Typically, processes at a single time scale but multiple length scales [1] or over a single length scale but multiple time scales [2] have been considered. In the present work, a generalized simultaneous prevalence of both multiple time and length scales is considered. Under a variety of circumstances, it is possible to examine the interaction of two processes, one of which operates at large time and large length scales and the other at small time and length scales (if the propagation speeds associated with the two processes are comparable), or more interestingly, one of which operates at large time and small length scales and the other at small time and large length scales (if the propagation speeds are markedly different). It is also known that fluid flows involve the simultaneous propagation of vortical, acoustic, and entropy waves [3]. In low Mach number situations, the acoustic waves would propagate at markedly different speeds than the rest. Particular attention is paid to this combination of time and length scale of two processes—flow and acoustic—as an interesting application of combustion thermoacoustics, where the mean flow Mach number is typically quite low.

Combustion dynamics is a serious practical problem in aero-engines and powerplants. The hallmark of this problem is the excitation of discrete acoustic tones of large amplitude under certain conditions

("combustion instability"). Correspondingly, the unsteady flame becomes highly compact under these conditions. Full compressible simulations of the combustor flow field can capture these features, but previous such works have not contrasted the conditions of combustion instability with what occurs in the near-absence of acoustic oscillations. Simpler theoretical analyses have always assumed the time scale of oscillatory combustion that acts as the acoustic source to be the same as that of the acoustic oscillations [4–6]. Many of these analyses adopt flame response/transfer functions that are evaluated by external excitation of a nominally stationary flame at low amplitudes. In reality, the flame intensely interacts with the acoustic oscillations it excites as the two processes evolve in time to limit cycle amplitudes. It is important not to assume equal time scales of the two processes a priori, and instead, show that the time scales approach each other under combustion instability conditions. It is also important to show that the flame evolves into a highly compact structure during these conditions, which has not been shown explicitly in previous works.

We consider two processes, one having a characteristic length scale L which is larger than the other h, and a characteristic time scale L/c_{ref} that is shorter than the other h/u_{ref} because $M = u_{ref}/c_{ref} << 1$, to begin with. The compressible Navier Stokes equation is decomposed by considering h/L and M as small quantites, into two sets, one each for the two processes considered; the procedure is detailed in section 2. The quantities and the equations can be recognized as those of viscous incompressible flow with temperature-dependent density flow for the short length/long time scale process and of inviscid compressible acoustic wave propagation for the large length/short time scale process. The eigenvalues of these equation sets show the respective convective speeds. The flow and acoustic velocities appear to leading order, the thermodynamic pressure is of zeroth order, the acoustic pressure is of first order, and the hydrodynamic pressure is of second order.

The set so obtained is tailored for the specific case of low Mach number and a smaller combustion zone embedded in a larger acoustic zone, in the context of thermoacoustic instabilities. This considers the simultaneous prevalence of multiple length- and time-scales, in general. Other asymptotic limits of single time-/multi-length and single length-/multi-time scales can be derived from this general set as particular cases derived earlier in the literature [1], [2]. Further more general sets of equations can be obtained for weakly compressible flows of multiple length and time scales. If the propagation speeds of the flow and acoustics are considered comparable, the combination of large length/large time and short length/short time scale processes can be modelled. In the extreme limit, we can retrieve fully compressible flow, with comparable length and time scales of flow and acoustics indistinguishably.

The present paper considers the specific case in the context of combustion thermoacoustics. The equations governing the base flow and acoustics in this regime are derived and the coupling terms between the two sets of equations are identified (section 2). The solution procedure to solve the coupled flow-acoustic equations are detailed in section 3. Numerical simulation of thermo-acoustic coupling in a backward-facing step combustor with fuel injection at the step corner is performed and the prominent results are discussed in section 4.

2 Mathematical Formulation

The schematic of the problem with specific context to a dump combustor is shown in Fig. 1. The flow/combustion field is modelled in a shorter length scale h and longer (convective) time scale $t = h/u_{ref}$, whereas the acoustics is modelled in a longer length scale L (for longitudinal acoustic modes) and shorter time scale $\tau = L/c_{ref}$. h is characteristic of the lateral dimensions of the combustor, such as the step height, and L is the length of the combustor. u_{ref} and c_{ref} are the reference flow and sound speeds.

The conservation equations are obtained after non-dimensionalising with shorter length and time scales, h and τ respectively. Reference quantities for mixture-density, velocity, pressure, temperature and partial-density of the K^{th} species are taken as ρ_{ref}, u_{ref}, p_{ref}, T_{ref} and $\rho_{K,ref}$ respectively. In the process, following dimensionless numbers are obtained: $Re = \rho_{ref} u_{ref} h/\mu$, $M = u_{ref}/c_{ref}$, $Pe = \rho_{ref} C_p u_{ref} h/\lambda$, $Da = \frac{Q_{ref} h}{p_{ref} u_{ref}}$, $Da_K = \frac{\omega_{ref} h}{\rho_{K,ref} u_{ref}}$ and $Sc = \frac{\mu}{\rho_{ref} D}$; Re, M, Pe, Da, Da_K and Sc are the Reynolds, Mach, Peclet, Damkohler, Damkohler (K^{th} species) and Schmidt numbers respectively. Q_{ref} and ω_{ref} are the reference heat release rate and species independent reaction rate, obtained at reference partial densities

of the species. μ, λ and C_p are the dynamic viscosity, thermal conductivity and specific heat at constant pressure of the fluid and are taken as constant. D is the species diffusivity, taken as equal and constant for all the species.

In the present work, M and h/L are taken to be small. To handle two small parameters simultaneously, each of them is in turn represented as a function of a single small number ε through the relations,

$$M = \varepsilon^m \tag{1}$$

and

$$\frac{h}{L} = \varepsilon^n. \tag{2}$$

Together, these constitute the simultaneous consideration of multiple length- and time-scales for any m and n. The resulting non-dimensional conservation equations are given below:

$$\frac{\partial \rho}{\partial \tau} + \varepsilon^{m-n} \frac{\partial}{\partial x_j} (\rho u_j) = 0 \tag{3}$$

$$\begin{aligned} \frac{\partial}{\partial \tau} (\rho u_i) + \varepsilon^{m-n} \frac{\partial}{\partial x_j} (\rho u_i u_j) + \varepsilon^{-(m+n)} \frac{1}{\gamma} \frac{\partial p}{\partial x_i} \\ = \varepsilon^{m-n} \frac{1}{Re} \left(\frac{\partial^2 u_i}{\partial x_j^2} + \frac{1}{3} \frac{\partial}{\partial x_i} \frac{\partial u_k}{\partial x_k} \right) \end{aligned} \tag{4}$$

$$\frac{\partial p}{\partial \tau} + \varepsilon^{m-n} \gamma \frac{\partial}{\partial x_j} (p u_j) = \varepsilon^{m-n} (\gamma - 1) Da Q_R + \varepsilon^{m-n} \frac{\gamma}{Pe} \frac{\partial^2 T}{\partial x_j^2} \tag{5}$$

$$\frac{\partial \rho_K}{\partial \tau} + \varepsilon^{m-n} \frac{\partial}{\partial x_j} (\rho_K u_j) = \frac{\varepsilon^{m-n}}{ReSc} \frac{\partial^2 \rho_K}{\partial x_j^2} + \varepsilon^{m-n} Da_K \omega_K \tag{6}$$

$$p = \rho T \tag{7}$$

ρ, u_j, p, T and ρ_K are the non-dimensional mixture-density, velocity, pressure, temperature and partial-density of the K^{th} species respectively. Q_R and ω_K are the non-dimensional heat release rate and production/depletion rate of the K^{th} species respectively.

We then expand any of the dependent variables ϕ according to the ansatz

$$\phi = \sum_{i=1,2,3,\ldots} \varepsilon^i \phi_i. \tag{8}$$

Splitting the spatial and temporal derivatives for the two scales considered as,

$$\frac{\partial}{\partial x} = \frac{\partial}{\partial x} + \frac{h}{L} \frac{\partial}{\partial \xi}, \tag{9}$$

$$\frac{\partial}{\partial \tau} = \frac{\partial}{\partial \tau} + \frac{ML}{h} \frac{\partial}{\partial t}, \tag{10}$$

and expanding the variables as powers of ε and comparing equi-order terms in ε, we decompose the conservation equations for the flow and acoustics in their respective length and time scales. The order of magnitude comparison also reveals the functional independence of certain variables which can be used in manipulating the equations. For instance, the leading order density, pressure and temperature (ρ_0, p_0 and T_0) do not depend on the shorter time scale τ; the leading order pressure p_0 does not have any spatial dependence and the first order pressure is not a function of shorter length scale.

The decomposed set of equations are given below,

Flow

$$\frac{\partial \rho_0}{\partial t} + \frac{\partial}{\partial x_{0,j}} (\rho_0 u_{0,j}) = 0 \tag{11}$$

$$\frac{\partial}{\partial t}\left(\rho_0 u_{0,i}\right) + \frac{\partial}{\partial x_j}\left(\rho_0 u_{0,i} u_{0,j}\right) = \frac{-1}{\gamma}\frac{\partial p_2}{\partial x_i} + \frac{1}{Re}\left(\frac{\partial^2 u_{0,i}}{\partial x_j^2} + \frac{1}{3}\frac{\partial}{\partial x_i}\left(\frac{\partial u_{0,k}}{\partial x_k}\right)\right) \tag{12}$$

$$\frac{dp_0}{dt} + \gamma p_0 \frac{\partial u_{0,j}}{\partial x_j} = (\gamma - 1) Da Q_{R,0} + \frac{\gamma}{Pe}\frac{\partial^2 T_0}{\partial x_j^2} \tag{13}$$

$$\frac{\partial \rho_{0,i}}{\partial t} + \frac{\partial}{\partial x_j}\left(\rho_{0,i} u_{0,j}\right) - \frac{1}{ReSc}\frac{\partial^2 \rho_{0,i}}{\partial x_j^2} - Da_i \omega_i = 0 \tag{14}$$

$$p_0 = \rho_0 T_0 \tag{15}$$

Acoustics

$$\frac{\partial \rho_1}{\partial \tau} + \frac{\partial}{\partial \xi_j}\left(\rho_0 u_{0,j}\right) = 0 \tag{16}$$

$$\rho_0 \frac{\partial u_{0,i}}{\partial \tau} + \frac{1}{\gamma}\frac{\partial p_1}{\partial \xi_i} = 0 \tag{17}$$

$$\frac{\partial p_1}{\partial \tau} + \gamma p_0 \frac{\partial u_{0,j}}{\partial \xi_j} = \frac{2\gamma}{Pe}\frac{\partial^2 T_0}{\partial x_j \partial \xi_j} \tag{18}$$

$$\frac{\partial \rho_{i,1}}{\partial \tau} + \frac{\partial}{\partial \xi_j}\left(\rho_{0,i} u_{0,j}\right) - \frac{2}{ReSc}\frac{\partial^2 \rho_{0,i}}{\partial x_j \xi_j} = 0 \tag{19}$$

$$p_1 = \rho_0 T_1 + \rho_1 T_0 \tag{20}$$

In the above set of equations, it is observed that both the flow and acoustics affect the fluid velocity to leading order. In this formulation, the acoustic variables are assumed to vary at longer length and shorter time scales and the flow variables at shorter length and longer time scales. Therefore, temporally averaging the base-flow equations (Eqs. 11-15) and spatially averaging the acoustic equations (Eqs. 16-20) results in the definition of new velocity variables that can be identified distinctly with the base flow and the acoustics. The averaging procedures are given below.

Temporal average $\overline{\phi}^{\tau}$ of a variable ϕ over the shorter time scale τ is defined as,

$$\overline{\phi}^{\tau}(x, \xi, t) = lim_{\epsilon \to 0} \frac{\epsilon}{t} \int_t \phi\left(x, \xi, t, \frac{t'}{\epsilon}\right) dt'$$

and ϕ can be written as,

$$\phi = \overline{\phi}^{\tau} + \phi'^{\tau}.$$

Similarly, spatial average $\overline{\phi}^{x}$ of a variable ϕ over the flow length scale h is defined as,

$$\overline{\phi}^{x}(\xi, \tau, t) = lim_{\epsilon \to 0} \frac{\epsilon^d}{V} \int_V \phi\left(\frac{\xi'}{\epsilon}, \xi, \tau, t\right) d^d\xi',$$

where d is the number of dimensions considered in space and V is the associated volume over which the integration is performed. ϕ can be written as,

$$\phi = \overline{\phi}^{x} + \phi'^{x}.$$

In the process, the leading order velocity variation at shorter time and length scale $u_0'^{\tau' x}$, the short length scale dependence of the first order density $\rho_1'^{x}$ and temperature $T_1'^{x}$ are assumed as unphysical and are set equal to zero. The final set of equations are given below,

Flow

$$\frac{\partial \rho_0}{\partial t} + \frac{\partial}{\partial x_j}\left(\rho_0 \overline{u_{0j}}^{\tau}\right) = 0 \tag{21}$$

$$\frac{\partial}{\partial t}\left(\rho_0 \overline{u_{0i}}^{\tau}\right) + \frac{\partial}{\partial x_j}\left(\rho_0 \overline{u_{0i}}^{\tau}\overline{u_{0j}}^{\tau}\right) + \frac{1}{\gamma}\frac{\partial \overline{p_2}^{\tau}}{\partial x_i} - \frac{1}{Re}\left(\frac{\partial^2 \overline{u_{0i}}^{\tau}}{\partial x_j^2} + \frac{1}{3}\frac{\partial}{\partial x_i}\left(\frac{\partial \overline{u_{0k}}^{\tau}}{\partial x_k}\right)\right) = -\frac{\partial}{\partial x_j}\left(\rho_0 \overline{u_{0i}'^{\tau} u_{0j}'^{\tau}}^{\tau}\right) \tag{22}$$

$$\frac{dp_0}{dt} + \gamma p_0 \frac{\partial \overline{u_{0,j}}^{\tau}}{\partial x_j} = (\gamma - 1) Da Q_{R,0} + \frac{\gamma}{Pe}\frac{\partial^2 T_0}{\partial x_j^2} \tag{23}$$

$$\frac{\partial \rho_{K,0}}{\partial t} + \frac{\partial}{\partial x_j}\left(\rho_{K,0}\overline{u_{0,j}}^{\tau}\right) - \frac{1}{ReSc}\frac{\partial^2 \rho_{K,0}}{\partial x_j^2} - Da_K \omega_K = 0 \tag{24}$$

$$p_0 = \rho_0 T_0 \tag{25}$$

Acoustics

$$\frac{\partial \rho_1}{\partial \tau} + \frac{\partial}{\partial \xi_j}\left(\overline{\rho_0}^{x} u_{0,j}'^{\tau}\right) = -\frac{\partial}{\partial \xi_j}\left(\overline{\rho_0}^{x}\overline{\overline{u_{0,j}}^{\tau}}^{x} + \overline{\rho_0'^{x}\overline{u_{0,j}}^{\tau}{}'^{x}}^{x}\right) \tag{26}$$

$$\overline{\rho_0}^{x}\frac{\partial u_{0,i}'^{\tau}}{\partial \tau} + \frac{1}{\gamma}\frac{\partial p_1}{\partial \xi_i} = 0 \tag{27}$$

$$\frac{\partial p_1}{\partial \tau} + \gamma p_0 \frac{\partial u_{0,j}'^{\tau}}{\partial \xi_j} = -\gamma p_0 \frac{\partial \overline{\overline{u_{0,j}}^{\tau}}^{x}}{\partial \xi_j} \tag{28}$$

$$\frac{\partial \overline{\rho_{K,1}}^{x}}{\partial \tau} + \frac{\partial}{\partial \xi_j}\left(\overline{\rho_{K,0}}^{x} u_{0,j}'^{\tau}\right) = -\frac{\partial}{\partial \xi_j}\left(\overline{\rho_{K,0}}^{x}\overline{\overline{u_{0,j}}^{\tau}}^{x} + \overline{\rho_{K,0}'^{x}\overline{u_{0,j}}^{\tau}{}'^{x}}^{x}\right) \tag{29}$$

$$p_1 = \rho_1 \overline{T_0}^{x} + \overline{\rho_0}^{x} T_1 \tag{30}$$

In these equations, we identify $\overline{u_{0,j}}^{\tau}$ as the flow velocity, and $u_{0,j}'^{\tau}$ as the acoustic velocity; and, $\overline{p_2}^{\tau}$ and p_1 as the hydrodynamic and acoustic pressures, respectively. With these variables, Eqs. (21) -(25) can be identified as the Navier-Stokes equations for incompressible flow with temperature-dependent density governing the combustion zone, and Eqs. (26)-(30) as the linearized Euler equations governing the acoustic zone. $Q_{R,0} = X_{O,0}^{a}\, X_{F,0}^{b} \exp^{-\frac{\theta}{T_0}}$ is used based on Arrhenius dependence of the reaction rate on temperature for a single step global chemical reaction with equal molecular weights assumed for all the species. Disregarding the species conservation for the moment in either the flow or the acoustic set of equations, we obtain three repeated eigenvalues namely, $\overline{u_{0,j}}^{\tau}$, i.e., the flow velocity, and two repeated eigenvalues equal to infinity for the flow set of equations in 3D. These are identified as corresponding to transport of vortical, entropy, and acoustic modes [3], with the speed of sound approaching infinity in the low Mach number limit. The acoustic equations yield two eigenvalues, namely $+c$ and $-c$, as appropriate for pure acoustic equations in the low Mach number limit. Considering that the acoustic set of equations has only two eigenvalues, only the acoustic momentum and energy conservation equations are solved.

Equations (21)-(30) can be used when $m = 1$ and $0 < n < 1$, for a simultaneous multi-length-time scale regime. Other asymptotic limits are already reported in the literature for single length scale and multiple time scale analysis [2], which can be obtained with $m = 1$, $n = 0$ in the above derivation; and for single-time-multiple-length scale analysis [1], which can be obtained with $m = n = 1$. For $n = 1$ and $0 < m < 1$, we would get equations for weakly compressible flows of multiple length and time scales. For $m = 0$, we would have comparable convective/propagation speeds of flow and acoustics, and hence the combination of large length/large time and short length/short time processes for $n \neq 0$. With both $m = n = 0$, we retrieve fully compressible flow, with comparable length and time scales of flow and acoustics indistinguishably.

In the multi-time-length scale regime represented by the above equations, it is observed that the spatio-temporal average of flow dilatation at the acoustic length scale acts as a source in the acoustic energy

balance equation (RHS of Eq. (28)), amplified by the mean pressure. This is the generalized source of acoustics emerging from the dilatation of the combustion zone. The fluctuation in heat release rate Q' used traditionally without regard for multiple length and time scales cannot be used in this regime. In the single-time-multiple-length scale limit, a similar derivation explicitly leads to $\overline{Q_{R,1}}^x$ as the acoustic source, i.e., the heat release fluctuations in the combustion zone that occur at the acoustic time scale averaged over the flow length scale, as if it is relatively a point source for the acoustics. For this, Eqs. (26), (29), and (30) are additionally to be used to calculate $\overline{Q_R 1}^x$ (not detailed here). For a single length scale, the acoustic source term is $Q'^{\tau}_{R,0}$. Since $Q_{R,0}$ varies only at the flow time scale, it does not contribute as source to acoustics unless the flow time scale and the acoustic time scale approach each other as conditions are varied.

The flow affects the acoustics through what appears to be the "acoustic Reynolds stress (ARS)" (RHS of Eq. (22)). Lighthill [7] identifies this term in the context of acoustic streaming, i.e., a mean flow induced by the acoustics by offering an average source of momentum, which with consideration of multiple scales is observed to affect the base flow. This term also appears in the single-length-multi-time scale regime ("average velocity tensor" [2]), but is replaced by the gradient in acoustic length scale of the acoustic pressure, a "pseudo-acceleration", in the single-time-multiple-length scale regime [1].

3 Solution Procedure

The flow set of equations (Eqs. 21-25) is numerically solved using the finite volume method with a semi-staggered grid arrangement. Simulations are reported for open combustion ($\frac{dp_0}{dt} = 0$). The energy balance equation (Eq. 23) reduces to a constraint equation on flow divergence, which the base flow velocity has to satisfy along with the momentum balance (Eq. 22). Pressure correction equation, similar to the one obtained for fully incompressible flow, can be derived using Eqs. 22 and 23. The base flow mass and species balance equations acts as a transport equation for mixture density and species partial densities respectively. The diffusion fluxes are discretized with second order accuracy. The convective fluxes are weighted between second order central and first order upwind schemes. The weightage to the upwind scheme is given as the cosine of the angle between the normal vector of the control surface and the flux vector crossing it. The solution is advanced in time in a iterative procedure similar to that of the SIMPLE scheme [8], which is close to being second order accurate in time [9]. The Poisson equation for pressure correction is solved using Fourier transform methods [10].

The acoustic set of equations is numerically solved using the open-source code CLAWPACK, a high-resolution multidimensional wave propagation solver [11], modified by us to handle multiple blocks and integrated to the in-house flow solver to solve the complete set of equations.

The flow domain is restricted to downstream of the step and extends up to a few flow length scales. The acoustic domain includes the flow domain and covers the entire length of the duct (Fig. 1). Flux boundary conditions are prescribed at the inlet to the flow domain; constant flux is specified for the fuel corresponding to choked flow from the fuel duct and the air mass flux is allowed to include net mass flow due to the acoustic velocity in an acoustic cycle. Outflow boundary condition is specified at the exit of the flow domain, where zero hydrodynamic pressure ($\overline{p_2}^{\tau}$) is prescribed and variation of all other flow variables across the boundary is taken as zero. The top and bottom surfaces are treated as walls. For acoustics, open-open boundary conditions are specified at the duct's inlet and exit boundaries (which are different from the inlet and exit boundaries of the flow domain). The top, bottom and step surfaces are treated as walls, where the no-penetration boundary condition is implemented.

The initial condition for the flow is the steady state flame, and that for the acoustics is quiescent, unless specifically stated otherwise. The flow length scale h is expected to vary as the system evolves from the initial steady state, because the flame shrinks as it progressively couples with the acoustic oscillations that it excites. Therefore, in our computations, the flow length scale is defined based on the heat release rate distribution in the domain. The heat release rate is integrated in the transverse direction through out the domain. The flow length scale is taken to be equal to the length for which the transversely integrated heat release rate gives 90% of the total heat release in the flow domain. This definition of the length scale serves the purpose of bringing in the variation of the flow length scale with change in operating conditions and the interaction between flow, combustion and acoustics. The change in the flow length scale alters the h/L ratio, and enables the time scales to approach each other towards instability in an

evolutionary manner from the initial conditions.

Typically, different time steps are taken for solving the flow and acoustics, but the spatial resolution of the acoustics is kept the same as that of the flow in the region where it overlaps with the flow (although it could be coarser) and it is decreased in the other regions as the variations to be resolved are of large length scale. The flow dilatation is spatially averaged over the flow length scale at every flow time step and supplied to all the acoustic time steps until it is updated at the next flow time step. The ARS is evaluated as a moving average in time over all the acoustic time steps within the acoustic time-scale (determined based on the natural frequency of the duct with the steady state flame) and supplied to the flow solver at every flow time step.

For the present work, the ratio of the step height to the duct length is taken as 0.01 and the ratio of the step to the inlet heights is taken as unity (Fig. 1). The mass fraction of the oxidizer at the air inlet is taken as 0.2 and that of the fuel is 0.52, with the rest taken as a diluent in both cases. The single step global reaction is typically patterned after a methane-air diffusion flame, with the molecular mass of all species involved taken equal as 40 based on mass conservation. Values used for the other non-dimensional parameters are: $Re = 585$, $M = 0.0003$, $Pe = 40$, $Da = 8.2 \times 10^{10}$, $Da_O = 2.1 \times 10^9$, $Da_F = 8.1 \times 10^8$, $\phi = 0.17$, $\theta = 48$, and $Le = 1$, where ϕ is the overall fuel-air equivalence ratio. The Reynolds number is varied in the range $292-2924$ in one set of test cases, so all the other related parameters change correspondingly in those cases. Grid independent solutions of the steady state flame are obtained for a grid spacing of 0.011. Grid spacing for the acoustics outside the flow domain is taken as 0.33, which is sufficient to capture the longitudinal acoustic waves.

4 Results and Discussion

As can be seen from the above formulation, variation of a large number of quantities is simultaneously involved during a simulation of flow-acoustic coupling. In the interest of space, variation of only one or two quantities are shown for each of the cases presented below.

First, the combustion-acoustic coupled simulations are attempted for the locations of the backward-facing step at $1/4^{th}$ and $3/4^{th}$ the distance from the duct entrance. The heat source located at quarter length is like the classical Rijke tube. Figure 2 shows the acoustic pressure fluctuations excited in the combustor as measured above the step for both locations of the step. It can be seen that the acoustics is excited to comparable levels in both cases. However, note that the $3/4^{th}$'s location excites oscillations of higher harmonic of the duct whereas the $1/4^{th}$'s location excites the fundamental frequency. This is exactly similar to that reported in [12], where an initial perturbation of the first mode was unstable for the $1/4^{th}$'s location whereas it was stable for the $3/4^{th}$ location but excited the higher harmonic even as it decayed.

The role of the ARS on the flow is significant. This is evaluated by comparing the cases when the ARS is retained in the flow-acoustic coupling versus when it is shut out, i.e., forced to zero at all times. The comparison is made in terms of the time evolution of the parameter n for the two cases in Fig. 3. n signifies the ratio of length scales, and hence is an indicator of the extent of how compact the flame evolves into during the instability. With $m = 1$ as in the present case, proximity of n to unity also signifies the flow and acoustic time scales approaching each other. For the laminar conditions considered here, the hydrodynamic instability time scale is not close to the acoustic time scale for realistic dimensions of the combustor length and step height. But, Fig. 3 shows how n grows towards unity within a small range from its initial value based on the steady state flame length, as the flame shrinks during the evolution of the flow-acoustic interaction, when the ARS contribution is retained. In contrast, the value of n remains nearly constant when the ARS contribution is suppressed.

The above discussion is best illustrated by the late-time evolution of the flame structure. Figure 4 compares the late-time instantaneous reaction rate fields at arbitrary instants for the two cases above. In the case where the ARS is suppressed, the flame undergoes a mild wavy motion about its steady state structure. On the other hand, with the ARS contribution retained, the flame undergoes enormous contortion that results from several micro folds in its structure during every acoustic time period, even as it retains its memory of these folds over the larger flow time scale. This results in a somewhat chaotic evolution of the flame structure after some time, which leads to most of its peak heat release occurring within a short region. These are the first results to the knowledge of the present authors that show

the evolution of a compact combustion zone as the system approaches combustion instability. Flame models that externally perturb the flame and consider its oscillations about its steady state structure are, therefore, likely to be erroneous in disregarding the above evolution. This can affect the transient growth of the oscillations during the evolution even when a system is deduced to be linearly stable at late times. In reality, turbulence in practical combustors would smear out the chaotic development and acoustic damping would lead to a limit cycle wherein the flame continues to fluctuate in a relatively compact zone. In the present formulation, viscous and conductive damping do not appear in the acoustic set of equations to leading order, and hence have not been included in the results shown above; thus, only the near-time evolutionary behaviour is resolved but late-time limit cycle amplitudes are not obtained, as in linear analyses.

Increasing the inlet air velocity into the combustor decreases the flow time scale through the combustion zone and makes it approach the acoustic time scale. The effect of a $10-$fold increase in the inlet air flow velocity, still in the laminar range, on the evolution of the parameter n, is shown in Fig. 5 along with several cases of intermediate inlet air velocities. As the inlet air velocity increases, the starting value of n obviously increases, but its sharp growth towards unity, signifying instability, occurs much sooner in the evolution of the flow-acoustic coupling. Correspondingly, the amplitude of the excited acoustic pressure increases with increase in the inlet air velocity, as observed in Fig. 6 for the above cases. The decrease in the time to instability (Fig. 5) as well as the increase in the amplitude (Fig. 6) level off after a sharp change with increase in the inlet air velocity. Notice also in Fig. 6 a slight decrease in the frequency of the excited acoustic pressure with increase in the inlet air velocity. This is typical of the base flow effect on the acoustic standing wave mode's frequency.

In all the above simulations, the acoustic damping is not taken into account. However, acoustic damping plays a critical role in limiting the amplitude of the acoustic oscillations. Acoustic damping predominantly occurs near the walls with the acoustic boundary layer, whose length scales are considerably lower than the flow length scales; therefore their contribution is not brought out in the acoustic balance equations (Eqs. 26-30). Considering the acoustic boundary layer in the solution will increase the computational cost considerably. Therefore, in order to explore the effect of damping in the evolution of the coupled system at reasonable computational cost, a visco-thermal friction term [13] is added to the acoustic momentum balance equation (Eq. 27); the resultant equation is given below,

$$\overline{\rho_0}^x \frac{\partial u'^{\tau}_{0,i}}{\partial \tau} + \frac{1}{\gamma}\frac{\partial p_1}{\partial \xi_i} = -2\alpha \overline{\rho_0}^x u'^{\tau}_{0,i}, \tag{31}$$

where, α, is the non-dimensional Helmholtz-Kirchhoff wall-attenuation coefficient [14], non-dimensionalized by the duct length L. In combustion flow fields, acoustic attenuation is increased due to the presence of water vapour [14]. This is approximately taken into account by increasing α up to five times the calculated value.

Considering acoustic attenuation limits the growth of acoustic amplitude as expected. Figure 7 shows the acoustic pressure monitored at the mid-y location of the inlet duct along the step plane. Decay in the acoustic pressure amplitude can be clearly seen, as compared to a nearly constant acoustic pressure amplitude when the acoustic attenuation is not taken into account (Fig. 2). After an initial decay spanning over a few acoustic cycles, the amplitude of the acoustic pressure increases sharply, due to a corresponding increase in the velocity divergence field of the base flow. As the coupled system is allowed to evolve in time, considerable vortex/flame roll-up and shedding is observed, as shown in Figure 8. These features are commonly observed in the operation of practical combustors and the coupled simulation based on the present formulation accounting acoustic attenuation in an approximate way is able to reproduce them.

5 Conclusion

A new approach is adopted to investigate combustion instability based on simultaneous consideration of multiple length and time scales of the flow/combustion and acoustic processes in the combustor. This involves the low Mach number approximation along with the combustion zone being shorter than the acoustic zone (for longitudinal acoustic modes). The decomposition of the governing equations for the combustion and acoustic zones results in the Navier-Stokes equations for incompressible flow with temperature-dependent density applicable in the former zone and the linearized Euler equations in the

latter, with additional source terms from each other. The flow dilatation acts as an acoustic energy source, and the acoustic Reynolds stress (ARS) acts as a source of the flow's momentum. Modifications to these terms previously published for single-length/multi-time and single-time/multi-length scales are retrieved from the present formulation in those limits. Considering temperature-dependent density is crucial to have the flow dilatation due to heat release as an acoustic source in this formulation. More importantly, the ARS is found to exert a history effect in chaotically contorting the flame as the flow-acoustic coupled system evolves from a steady, quiescent state towards combustion instability; the flame becomes progressively compact as observed experimentally. These features cannot be brought out in flame models that consider external excitation of a flame about its steady state. The parameter n grows towards unity as the flame shrinks, signifying that the flow and acoustic time scales approach each other, in the low Mach number limit. Flame/vortex roll-up and its shedding is observed when the coupled simulation is continued for extended time with acoustic damping taken into account. As such, numerical simulations for a model problem of laminar 2D nonpremixed flame in a dump combustor reported here show the spontaneous, simultaneous, transient growths in the amplitudes of a collection of acoustic modes at near times from the start of flow-acoustic coupling. The approach also marks substantial cost savings relative to computing the full 3D compressible flow equations over the full combustor domain to resolve acoustic oscillations that are 1D for most part and of small amplitude and fluctuating at a small time-scale superposed over the larger base flow variations at larger time scales in a small region.

References

[1] R. Klein, ESAIM:M2AN 39 (2005) 537-559.

[2] B. Muller, J. Eng. Math 34 (1998) 97-109.

[3] B. -T. Chu, L. S. G. Kovaznay, J. Fluid Mech. 3 (1958) 494-514.

[4] A. P. Dowling, S. R. Stow, J. Propul. Power 19 (5) (2003) 751-764.

[5] G. J. Bloxsidge, A. P. Dowling, P. J. Langhorne, J. Fluid Mech. 193 (1988) 445-473.

[6] T. Schuller, D. Durox, S. Candel, Combustion and Flame 135 (2003) 525–537.

[7] J. Lighthill, J. Sound Vib. 61 (3) (1978) 391-418.

[8] S. V. Patankar, Numerical heat transfer and fluid flow (1980) New York: Hemisphere Publishing Corporation.

[9] V. Raghavan, V. Babu, T. Sundararajan, R. Natarajan, Int. J. Heat and Mass Transfer 48 (2005) 5354-5370.

[10] W. H. Press, S. A. Teukolsky, W. T. Vetterling, B. P. Flannery, Numerical Recipes in C The Art of Scientific Computing 3^{rd} edition (2007) Singapore: Cambridge University Press.

[11] R. J. Leveque, J. Comp. Phys. 131 (1997) 327-353.

[12] M. Tyagi, S. R. Chakravarthy, R. I. Sujith, Combust. Theo. Modell. 11 (2) (2007) 205-226.

[13] S. N. Rschevkin, A Course of Lectures on the Theory of Sound (1963) Mcmillan, New York.

[14] S. Temkin, Elements of Acoustics (1981) John Wiley and Sons, New York.

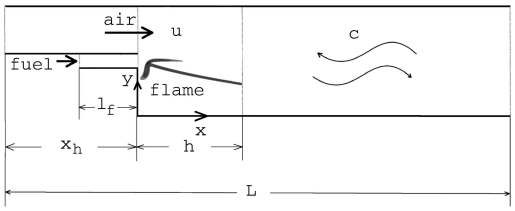

Figure 1: Schematic of the combustor.

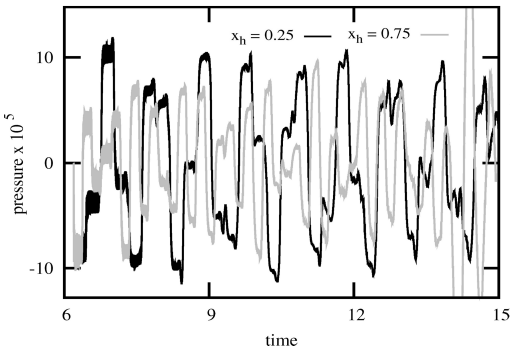

Figure 2: Evolution of acoustic pressure for two different axial locations of the step in the combustor.

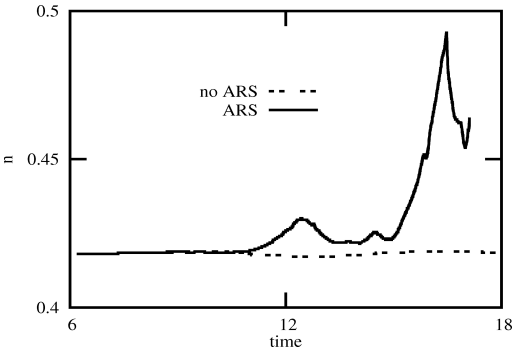

Figure 3: Effect of the acoustic Reynolds stress (ARS) on the evolution of the parameter n.

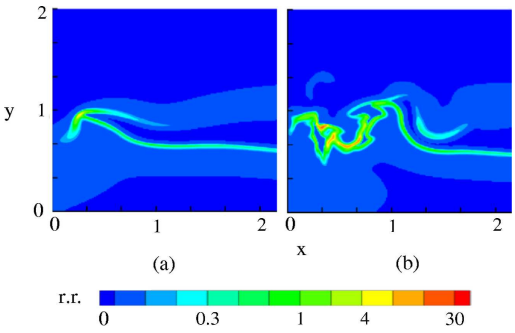

Figure 4: Effect of the acoustic Reynolds stress (ARS) on the late-time evolution of the reaction rate distribution in the combustion zone; (a) without ARS, (b) with ARS.

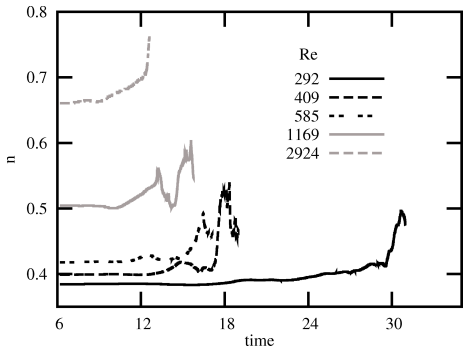

Figure 5: Effect of inlet air Reynolds number on the evolution of parameter n during flow-acoustic coupling.

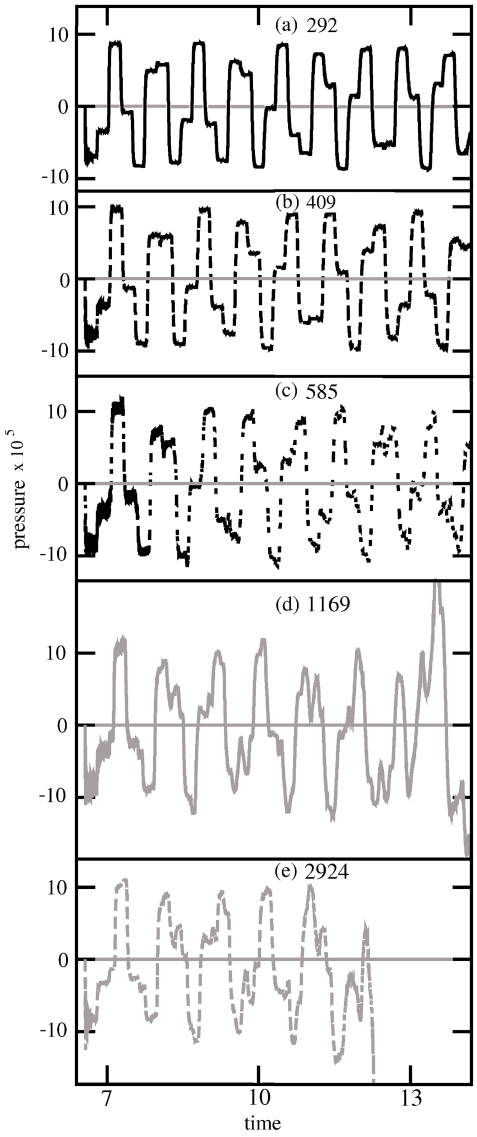

Figure 6: Evolution of acoustic pressure for different inlet air Reynolds numbers.

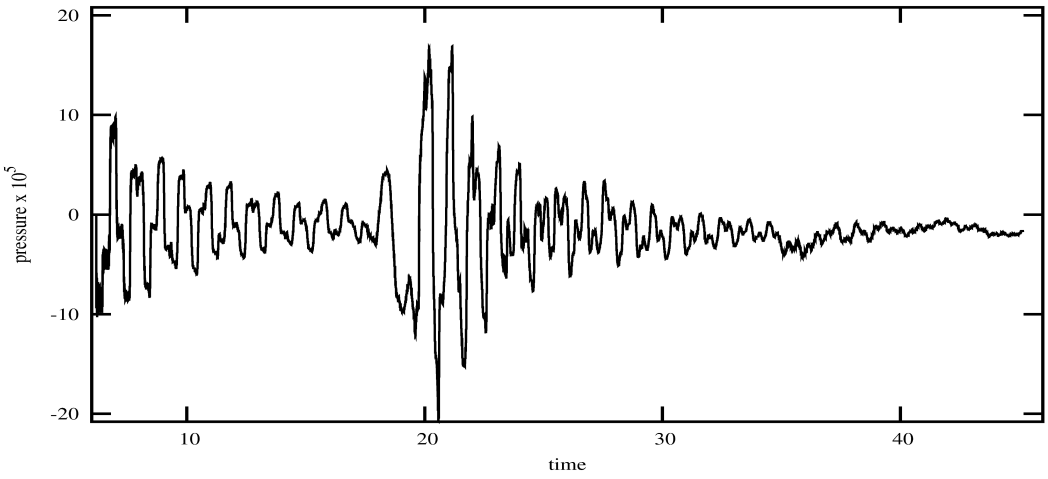

Figure 7: Evolution of acoustic pressure with acoustic damping.

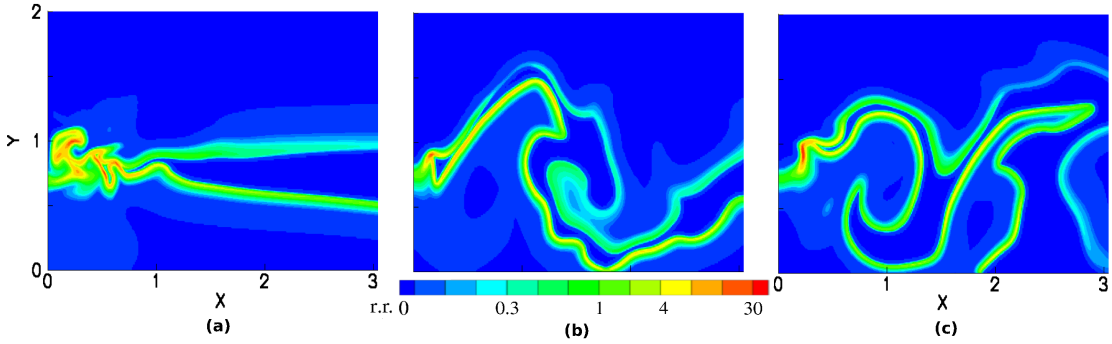

Figure 8: Flame roll-up due to flame-acoustic interaction. The figures are separated by 13 acoustic cycles. Initial concatenation of small vortical structures (a) results in roll-up of large structure (b) and its subsequent shedding (c).